RESEARCH ARTICLE

Integrin-α10 Dependency Identifies RAC and RICTOR as Therapeutic Targets in High-Grade Myxofibrosarcoma

Tomoyo Okada[1], Ann Y. Lee[1], Li-Xuan Qin[2], Narasimhan Agaram[3], Takahiro Mimae[1], Yawei Shen[1], Rachael O'Connor[1], Miguel A. López-Lago[4], Amanda Craig[1], Martin L. Miller[5], Phaedra Agius[1], Evan Molinelli[5], Nicholas D. Socci[5], Aimee M. Crago[1,6], Fumi Shima[7], Chris Sander[5], and Samuel Singer[1,6]

ABSTRACT Myxofibrosarcoma is a common mesenchymal malignancy with complex genomics and heterogeneous clinical outcomes. Through gene-expression profiling of 64 primary high-grade myxofibrosarcomas, we defined an expression signature associated with clinical outcome. The gene most significantly associated with disease-specific death and distant metastasis was *ITGA10* (integrin-α10). Functional studies revealed that myxofibrosarcoma cells strongly depended on integrin-α10, whereas normal mesenchymal cells did not. Integrin-α10 transmitted its tumor-specific signal via TRIO and RICTOR, two oncoproteins that are frequently co-overexpressed through gene amplification on chromosome 5p. TRIO and RICTOR activated RAC/PAK and AKT/mTOR to promote sarcoma cell survival. Inhibition of these proteins with EHop-016 (RAC inhibitor) and INK128 (mTOR inhibitor) had antitumor effects in tumor-derived cell lines and mouse xenografts, and combining the drugs enhanced the effects. Our results demonstrate the importance of integrin-α10/TRIO/RICTOR signaling for driving myxofibrosarcoma progression and provide the basis for promising targeted treatment strategies for patients with high-risk disease.

SIGNIFICANCE: Identifying the molecular pathogenesis for myxofibrosarcoma progression has proven challenging given the highly complex genomic alterations in this tumor type. We found that integrin-α10 promotes tumor cell survival through activation of TRIO–RAC–RICTOR–mTOR signaling, and that inhibitors of RAC and mTOR have antitumor effects *in vivo*, thus identifying a potential treatment strategy for patients with high-risk myxofibrosarcoma. *Cancer Discov; 6(10); 1148–65. ©2016 AACR.*

INTRODUCTION

Myxofibrosarcoma is one of the most common histologic types of soft-tissue sarcoma in adults, typically occurring in the extremities. Formerly known as a myxoid variant of malignant fibrous histiocytoma (a classification representing undifferentiated pleomorphic sarcomas), myxofibrosarcoma is currently regarded as a distinct fibroblastic/myofibroblastic tumor type defined by cellular pleomorphism, a curvilinear vascular pattern, and a myxoid stromal component (1–3). Although the mainstay of therapy is surgical resection, and 5-year disease-specific survival (DSS) after surgery for primary high-grade myxofibrosarcoma is 60% to 70%, approximately 30% to 40% of high-grade tumors metastasize to lung, bone, or lymph nodes (4–7). Once myxofibrosarcoma has metastasized, conventional chemotherapy and radiation therapy are largely palliative, and metastasis eventually leads to disease-related death.

Prior genomic studies of myxofibrosarcoma have revealed no single characteristic genetic alteration; instead, single-nucleotide polymorphism (SNP) and array comparative genomic hybridization (CGH) studies have shown that myxofibrosarcoma is among the most highly complex sarcoma types (8–10). The gene most commonly mutated was *NF1*, mutated in 10.5% of myxofibrosarcomas. The most common copy-number gain/amplification was on 5p, occurring in 60% of myxofibrosarcomas (8). Among the genes in this amplicon, *TRIO*, *SKP2*, and *AMACR* were shown to be overexpressed, and *SKP2* and *AMACR* were found to be potential oncogenes in myxofibrosarcoma (11, 12). It remains unclear whether any other genes in the 5p amplicon serve as critical drivers in myxofibrosarcoma. Because of the genetic and karyotypic complexity, defining the molecular pathogenesis underlying metastatic myxofibrosarcoma has been challenging and we still lack targeted therapies against specific oncogenic pathways for this deadly sarcoma (10, 13).

Integrins are cell-surface receptors that mediate the interaction of cells with the microenvironment through binding to their ligands, extracellular matrix (ECM) proteins. Upon ligand binding, activated integrins promote cellular adhesion and interact directly or indirectly with a number of proteins

[1]Sarcoma Biology Laboratory, Sarcoma Disease Management Program, Department of Surgery, Memorial Sloan Kettering Cancer Center, New York, New York. [2]Department of Biostatistics, Memorial Sloan Kettering Cancer Center, New York, New York. [3]Department of Pathology, Memorial Sloan Kettering Cancer Center, New York, New York. [4]Department of Surgery, Memorial Sloan Kettering Cancer Center, New York, New York. [5]Computational Biology Center, Memorial Sloan Kettering Cancer Center, New York, New York. [6]Department of Surgery, Weill Cornell Medical College, New York, New York. [7]Graduate School of Science, Technology and Innovation, Kobe University, Kobe, Japan.

Note: Supplementary data for this article are available at Cancer Discovery Online (http://cancerdiscovery.aacrjournals.org/).

T. Okada and A.Y. Lee contributed equally to this article.

Current address for A.Y. Lee: New York University School of Medicine, New York, New York; current address for A. Craig: Department of Medicine, Icahn School of Medicine at Mount Sinai, New York, New York; current address for M.L. Miller: University of Cambridge, Cancer Research UK, Cambridge Institute, UK; current address for P. Agius: New York Genome Center, New York, New York; current address for E. Molinelli: BioDigital, Inc., New York, New York; and current address for C. Sander: cBio Center at Dana-Farber Cancer Institute and Department of Cell Biology, Harvard Medical School, Boston, Massachusetts.

Corresponding Authors: Samuel Singer, Memorial Sloan Kettering Cancer Center, 1275 York Avenue, Howard 1205, New York, NY 10065. Phone: 212-639-2940; Fax: 646-422-2300; E-mail: singers@mskcc.org; and Tomoyo Okada, Zuckerman Research Center, Memorial Sloan Kettering Cancer Center, 417 East 68th Street, ZRC445B, New York, NY 10065. Phone: 646-888-3205; E-mail: t-okada@ski.mskcc.org

doi: 10.1158/2159-8290.CD-15-1481

to initiate cellular signaling for proliferation, migration, and survival (14). Integrins are heterodimers composed of an alpha and a beta subunit. Some aspects of ECM-integrin signaling are known to be dysregulated in cancers, with pro-malignant consequences such as promotion of stemness, survival in stressful environments, enhanced angiogenesis, resistance to chemotherapy, and distant metastasis (15). Although integrins alone do not transform cells, some of the pro-malignant integrins associate with and signal through oncoproteins, such as SRC, FAK, and receptor tyrosine kinases (16, 17).

Integrin-α10, isolated as a collagen II–binding integrin from chondrocytes (18), is the alpha subunit of one of the collagen II–receptor integrins (integrins α1β1, α2β1, and α10β1). Integrin-α10 shows a restricted tissue expression pattern, most abundant in cartilage-containing tissues but also in fibrous tissues such as the fascia lining skeletal muscle fibers (19). Integrin α10β1 is known from knockout studies to be essential for growth plate formation during skeletal development (20). Data are scarce on the role of integrin-α10 in human cancer. Integrin-α10 is overexpressed in primary and metastatic melanoma cells and is associated with melanoma cell migration (21). In contrast, in several other solid tumors, the downregulation of integrin-α10 is associated with loss of phosphorylated RB and with disease progression (22). These results suggest that the role of integrin-α10 in human cancer is context dependent. The role of integrin-α10 in sarcomagenesis remains unknown.

To investigate the molecular basis of myxofibrosarcoma oncogenesis and progression, we undertook gene expression profiling of a well-characterized set of 64 primary untreated high-grade myxofibrosarcomas. Unsupervised clustering identified a subgroup associated with poor clinical outcome. This subgroup had strikingly higher expression of the integrin-α10 gene *ITGA10*, and its expression was also independently associated with outcome. We therefore investigated the role of integrin-α10 in myxofibrosarcoma cells, defined the pathways by which it exerts its effects, and tested pharmacologic inhibition of these pathways for antitumor effects both *in vitro* and *in vivo*.

RESULTS

Gene Expression Profiles Define Two Molecular Subtypes of Myxofibrosarcoma

U133A microarray data were obtained for 64 primary untreated high-grade myxofibrosarcomas; their characteristics are shown in Supplementary Table S1. The median tumor size was 8.5 cm, and 81% of tumors were deep. The median percent myxoid component was 75% (range, 10%–100%). At a median follow-up of 2.6 years, 22% of the patients had a local recurrence, 34% developed metastases, and 27% ultimately died of disease. All patients who died of disease had developed metastases, and all died within 3.5 years of their initial surgery. Unsupervised consensus clustering of the microarray data grouped myxofibrosarcomas into two clusters (Fig. 1A). Similar myxofibrosarcoma clusters arose in an analysis that also included normal fat and normal muscle tissue, and the normal samples were all well separated from the myxofibrosarcomas (Supplementary Fig. S1A). Cluster 1 patients showed significantly worse DSS than cluster 2 patients (Fig. 1B; $P = 0.021$). To further test the importance of this grouping, we performed a multivariate analysis adjusting for tumor size, the most important known clinical predictor in myxofibrosarcoma (4, 23–25). Both variables were independent predictors of DSS: tumor size as a continuous variable had a hazard ratio of 1.15 ($P = 0.010$), and cluster 1 versus cluster 2 membership had a hazard ratio of 5.26 ($P = 0.014$).

There were 2,366 gene probes differentially expressed (at $P < 0.001$) between the two clusters (Supplementary Table S2). Of these 2,366 probes, 186 (representing 146 genes) were also significantly associated with DSS at $P < 0.005$ (Fig. 1C and D; see the full list in Supplementary Table S3). For 6 of the top-ranked genes, we remeasured expression by quantitative PCR and validated the associations with survival (Fig. 1E; Supplementary Fig. S1B).

To provide biological context to the 146 survival-associated genes, we used the NetBox algorithm (26) to analyze pathways. This algorithm identifies modules of interconnected genes from known human protein–protein and signal transduction pathway interactions. Using the 146 genes as input, NetBox identified 15 pathway modules, which exhibited a stronger degree of connectedness (modularity) than expected by chance (Fig. 1F; Supplementary Table S4). Among the modules with five or more members, gene-annotation analysis with the DAVID tool (27) revealed enrichment for functional annotations related to cell–ECM interactions such as "Focal Adhesion," "Extracellular Matrix," and "Plasma Membrane" (Fig. 1F; Supplementary Table S5). The top-scoring pathway module, M0, contained an interconnected set of integrins.

Among the 146 differentially expressed genes associated with DSS, the most strongly associated was *ITGA10*, which encodes integrin-α10 (hazard ratio 2.46; $P = 0.000003$). *ITGA10* mRNA was also significantly associated with distant recurrence-free survival (hazard ratio 3.75; $P = 0.001$; Fig. 1E). For 5 patients we had samples of metastases as well as the primary tumor; 4 of the 5 had higher *ITGA10* mRNA in the metastasis (Fig. 1G). *ITGA10* mRNA was significantly higher in the metastases in a larger set of unmatched samples ($P = 0.003$; Fig. 1G). Based on these findings, we chose *ITGA10* for functional analysis.

Silencing of Integrin-α10 Induces Growth Suppression through Apoptosis in Myxofibrosarcoma Cells but Not in Normal Mesenchymal Cells

To examine whether integrin-α10 is a driver gene for myxofibrosarcoma, we undertook knockdown studies of integrin-α10 in myxofibrosarcoma cell lines. First, we investigated the expression of *ITGA10* mRNA in four different cell lines established from myxofibrosarcoma tumor tissues, together with adipose-derived mesenchymal stem cells (ASC) and three other normal human mesenchymal cell types. Three of the four myxofibrosarcoma cell lines exhibited high *ITGA10* mRNA levels compared with any of the normal mesenchymal cells (Supplementary Fig. S2A). Two independent shRNA constructs knocked down integrin-α10 expression efficiently (Supplementary Fig. S2B and S2C). Both shRNAs robustly suppressed cell growth and induced apoptosis in the myxofibrosarcoma cell lines, but not ASCs, SGBS, or KEL-FIB (Fig. 2A–C; Supplementary Fig. S2D and S2E). Interestingly, knockdown induced growth suppression and apoptosis in all four myxofibrosarcoma cell lines, including the one with relatively low *ITGA10* expression (MXF8500). Thus, integrin-α10

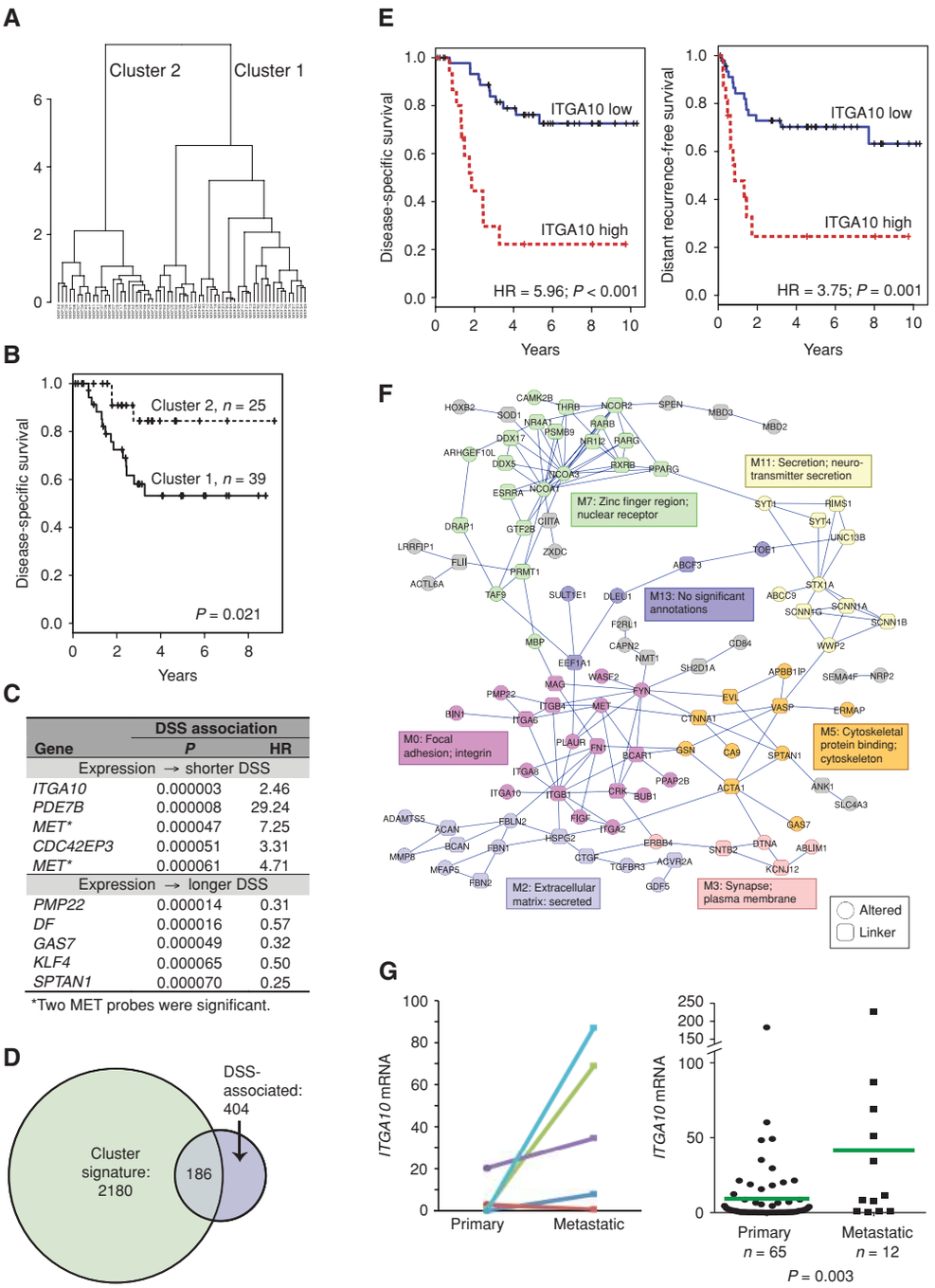

Gene	DSS association P	HR
Expression → shorter DSS		
ITGA10	0.000003	2.46
PDE7B	0.000008	29.24
*MET**	0.000047	7.25
CDC42EP3	0.000051	3.31
*MET**	0.000061	4.71
Expression → longer DSS		
PMP22	0.000014	0.31
DF	0.000016	0.57
GAS7	0.000049	0.32
KLF4	0.000065	0.50
SPTAN1	0.000070	0.25

*Two MET probes were significant.

Figure 1. Unsupervised clustering and genes associated with survival of patients with myxofibrosarcoma. **A,** unsupervised clustering of U133A microarray data for 64 untreated primary high-grade myxofibrosarcoma samples. The clustering results are based on consensus clustering, and the distance measure reflects co-clustering frequency. **B,** Kaplan–Meier curves comparing disease-specific survival (DSS) of cluster 1 vs. cluster 2. **C,** the genes whose probes were most significantly associated with DSS among the cluster signature gene probes. The hazard ratio (HR) represents the HR per unit increase in expression value when expression is treated as a continuous variable. **D,** Venn diagram showing overlap between gene probes that were differentially expressed between clusters 1 and 2 and gene probes whose expression was independently associated with DSS. In total, 22,215 probes were analyzed. **E,** Kaplan–Meier curves comparing DSS (top) distant recurrence–free survival (bottom) of patients with low vs. high *ITGA10* mRNA levels measured by quantitative PCR. **F,** pathway modules identified by NetBox analysis of the 146 genes that were both in the cluster signature and associated with DSS. Fifty-four of the genes (circles) were found in the background protein–protein interaction network, and they could be interconnected through an extracted set of 48 "linker" genes (squares) that were statistically enriched for interactions with the input genes. Modules with five or more members were color coded and annotated based on enrichment analysis using the DAVID tool. The remaining genes are colored gray. **G,** levels of *ITGA10* mRNA from primary and metastatic tumors. The values shown are relative to the value in ASCs. Left, matched samples from 5 patients; right, all samples analyzed (including the matched samples). Characteristics of the patients are shown in Supplementary Table S7.

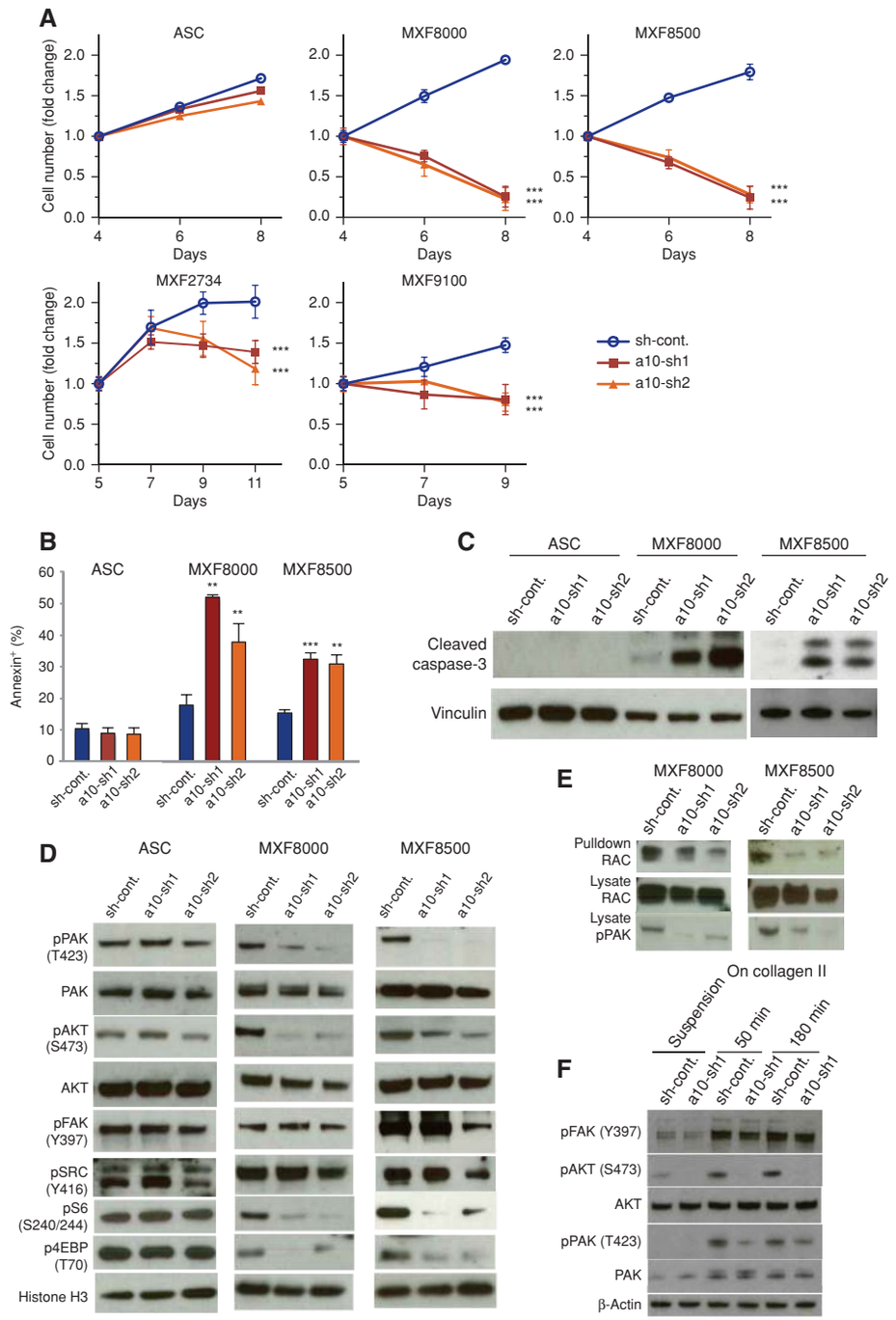

Figure 2. Integrin-α10 is required for cell growth and activation of AKT and RAC/PAK in myxofibrosarcoma cells but not in mesenchymal stem cells. To knock down integrin-α10, we infected adipose-derived mesenchymal stem cells (ASC) or tumor-derived myxofibrosarcoma cell lines with lentivirus encoding either of two shRNAs against integrin-α10 (a10-sh1 and a10-sh2) or scramble shRNA (sh-cont.). **A,** proliferation of myxofibrosarcoma cells lines and normal cells after integrin-α10 knockdown. Equal numbers of cells were plated on day 4 or 5 after lentivirus infection, and cell viabilities were quantified at the indicated time points. The plots show fold change (mean ± SD; $n = 6$) relative to the day of plating. Error bars in these and other graphs indicate standard deviation. **B** and **C,** apoptosis after integrin-α10 knockdown. Apoptosis was assessed by the percentage of annexin (+) cells in triplicate cultures (**B**) or by immunoblot to detect cleaved caspase-3 (**C**). **D,** effect of integrin-α10 knockdown on signaling proteins. Total protein from integrin-α10-knockdown cells or control cells (after 8–10 days of infection) was subjected to immunoblotting with the indicated antibodies. **E,** effect of integrin-α10 knockdown on collagen II adhesion-dependent signaling. MXF8000 cells with either control or integrin-α10 shRNA were detached, resuspended in serum-free medium, and either kept in suspension or replated onto collagen II–coated dishes for the indicated times. Total lysates were subjected to immunoblotting with the indicated antibodies. **F,** effect of integrin-α10 knockdown on RAC activation. In lysates of MXF8000 and MXF8500 cells with integrin-α10 shRNA or control shRNA, GTP-RAC was detected by pulldown using GST-RBD, followed by immunoblotting. The same lysates were also immunoblotted with antibody against total RAC and phospho-PAK (pPAK). In this and other figures, asterisks indicate statistical significance by the Student *t* test: *, $P < 0.05$; **, $P < 0.01$; ***, $P < 0.001$.

is required for growth and survival of these myxofibrosarcoma cells but is dispensable for normal mesenchymal-derived cells, indicating that integrin-α10 plays a tumor-specific role.

Forced Expression of Integrin-α10 Enhances Cell Migration and Invasion

To examine the effects of integrin-α10 on metastatic traits, we overexpressed it in SV40-transformed ASCs. As shown in Supplementary Fig. S2F and S2G, cells overexpressing integrin-α10 exhibited greater migration and invasion through Matrigel than the control cells.

Integrin-α10 Regulates the Activities of RAC/PAK and AKT in Myxofibrosarcoma

To explore the downstream signaling events responsible for the myxofibrosarcoma-specific role of integrin-α10, we examined pathways known to mediate integrin signaling. After knockdown of *ITGA10*, we observed significant downregulation of the activation of both PAK (T423 phosphorylation) and AKT (S473 phosphorylation; Fig. 2D). Activation of SRC and FAK, however, was not consistently affected. To examine the PAK pathway further, we examined its upstream regulator RAC, assessing levels of activated (GTP-bound) RAC by its ability to bind the p21-binding domain of PAK in a pulldown assay. This experiment confirmed that integrin-α10 knockdown inhibited RAC activation (Fig. 2E). Notably, neither AKT nor PAK was inhibited in ASCs, indicating that these cells do not need integrin-α10 for the activation of AKT and RAC/PAK. Because AKT is an upstream activator of the protein complex mTORC1, we also examined the effects of integrin-α10 silencing on the two major targets of mTORC1, phospho-S6 and phospho-4EBP, and found that the silencing reduced the levels of these phosphoproteins in myxofibrosarcoma cells but not in ASCs (Fig. 2D).

To examine the effects of integrin-α10 on adhesion-dependent signaling in myxofibrosarcoma cells, we compared cells with and without integrin-α10 when plated on collagen II versus in suspension. Plating on collagen II induced activation of FAK, AKT, and PAK, and the integrin-α10 knockdown abolished this activation of AKT and PAK, but not of FAK (Fig. 2F). These results suggest that upon binding to the extracellular matrix, integrin-α10 engages in tumor-specific signaling to activate RAC/PAK and AKT/mTORC1.

Because *ITGA10* knockdown induced growth suppression and apoptosis in cells that showed no obvious detachment, we hypothesized that the cell death was not caused by loss of adhesion. We therefore directly assessed the effect of *ITGA10* knockdown on adhesion to collagen I and collagen II. The *ITGA10*-knockdown cells adhered to both collagens as efficiently as the control shRNA cells (Supplementary Fig. S3A). The preserved adhesion in *ITGA10*-knockdown cells was also confirmed by immunostaining to detect phospho-FAK and vinculin at focal adhesion sites (Supplementary Fig. S3B). Integrin-α10 overexpressed through lentivirus transduction in myxofibrosarcoma cells was consistently found to diffusely localize to the plasma membranes and some lamellipodia, but did not colocalize with vinculin or phospho-FAK at the typical focal adhesion structures (Supplementary Fig. S3C). Thus, high expression of integrin-α10 is not required for myxofibrosarcoma cells' adhesion to the collagen II matrix. In fact, myxofibrosarcoma cells express two other collagen II–binding integrins, integrin-α1 and integrin-α2, at the cell surface, as detected by FACS (data not shown). To further examine the specific requirement of integrin-α10 on myxofibrosarcoma cell survival signaling through AKT and PAK, we knocked down integrin-α1 and integrin-α2. Knockdown of either integrin-α1 or integrin-α2 did not induce apoptosis and did not inhibit PAK or AKT activation (Supplementary Fig. S3D and S2E). These data demonstrated the specific requirement of integrin-α10 signaling via PAK and AKT for the survival of myxofibrosarcoma cells.

TRIO and RICTOR Are Overexpressed via DNA Amplification in Myxofibrosarcoma and Physically Associate with Integrin-α10

To search for genes that might connect integrin-α10 to the activities of RAC and AKT, we analyzed array CGH data from the patients. The recurrent chromosome 5p amplicon (Fig. 3A) contains two genes that appeared relevant, *TRIO* and *RICTOR*. TRIO is a guanine nucleotide exchange factor that facilitates the activation of RAC, and RICTOR is an essential component of mTORC2, which is the major kinase for S473 of AKT. In our array CGH data, we found that nearly half of the tumors (27 of 64; 42%) possessed coamplification of *TRIO* and *RICTOR* (Supplementary Fig. S4A). Coamplification was significantly associated with worse DSS (Supplementary Fig. S4B). Because U133A arrays lack a probe for *RICTOR*, we used quantitative PCR to determine *RICTOR* and *TRIO* mRNA levels in the 64 myxofibrosarcoma samples. Both *RICTOR* and *TRIO* mRNA levels were positively associated with copy number of the genes (Fig. 3B), and the two mRNAs were correlated with each other (Supplementary Fig. S4C). Although in the overall study group expression levels of *TRIO* and *RICTOR* were not significantly associated with outcomes, for the subset whose tumors had high *ITGA10* expression ($n = 32$), high *TRIO* expression was significantly associated with worse DSS and distant recurrence–free survival, as was combined expression of *TRIO* and *RICTOR* (Fig. 3C; Supplementary Fig. S4D). Taken together, these data further support the oncogenic link between integrin-α10 and TRIO/RICTOR (28). Mirroring our findings in myxofibrosarcoma tissue, we found *TRIO* and *RICTOR* amplifications in our myxofibrosarcoma cell lines, and expression of *TRIO* and *RICTOR* was increased at both mRNA and protein levels in the four myxofibrosarcoma cell lines compared with the four normal mesenchymal cell types (Fig. 3D and E).

Given these findings, we hypothesized that integrin-α10 signals through TRIO for the control of RAC and through RICTOR for the control of AKT. We therefore tested whether, following ligand binding, integrin-α10 binds to TRIO and RICTOR. In lysates of MXF8000 cells exposed to collagen II, antibody against integrin-α10, but not control rabbit IgG, precipitated integrin-α10 together with TRIO and RICTOR (Fig. 3F). Importantly, RAPTOR, a TORC1 component, was not precipitated, further supporting the specificity of the immunoprecipitation. Thus, activated integrin-α10 exposed to ligand forms complexes with TRIO and RICTOR.

TRIO and RAC Are Required for Growth of Myxofibrosarcoma Cells

To assess the contributions of TRIO and its direct target RAC1 to the integrin-α10–mediated growth signal, we used lentivirus-based shRNA knockdown of TRIO and RAC1 in

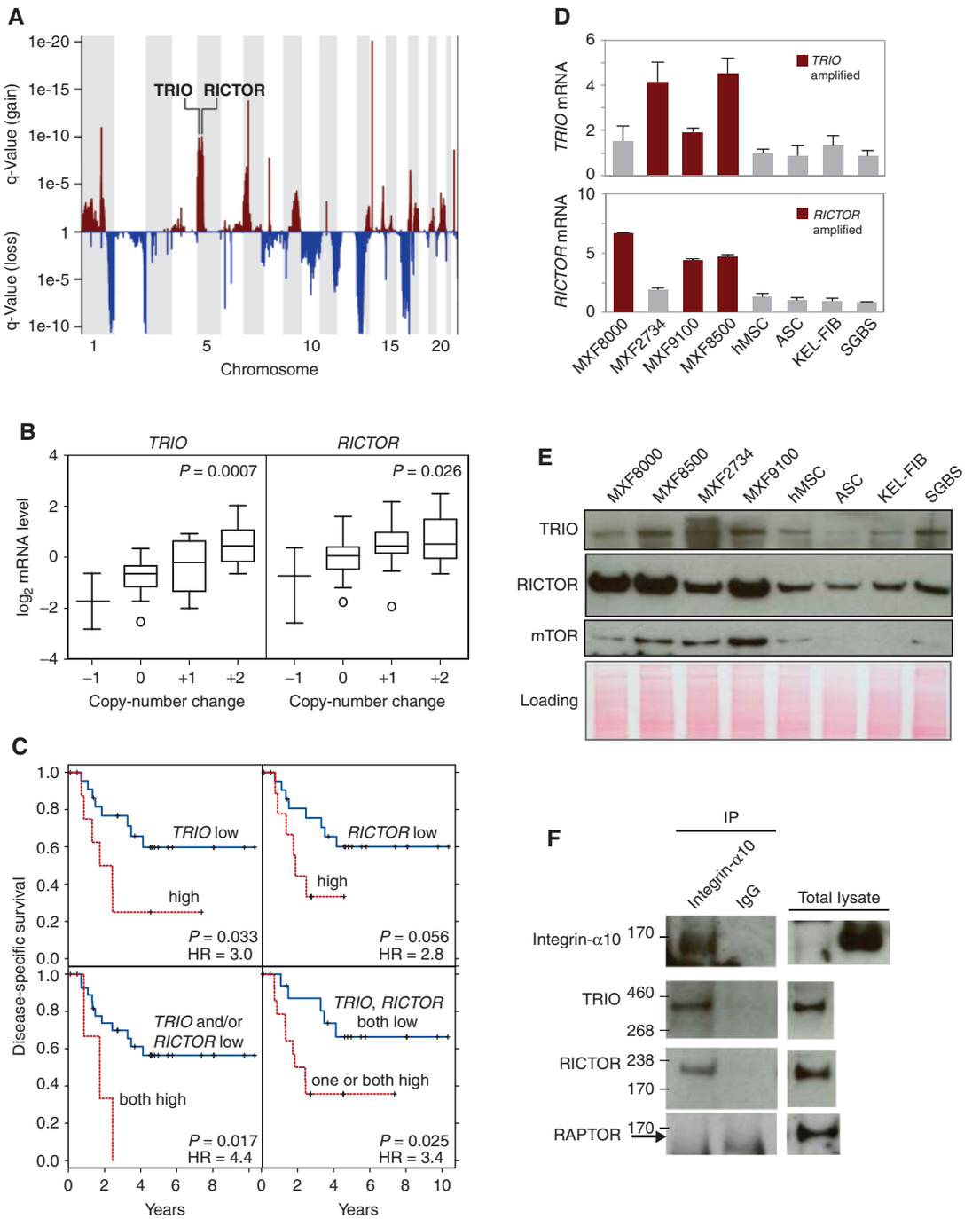

Figure 3. Gene amplification and overexpression of *TRIO* and *RICTOR* in myxofibrosarcoma tumor tissues and cell lines. **A,** copy-number alterations in myxofibrosarcoma. The graph shows the statistical significance of copy-number gain (red) or loss (blue). Black lines indicate the loci of *TRIO* and *RICTOR* on chromosome 5p. **B,** elevated expression of *TRIO* and *RICTOR* associated with copy-number amplification. mRNA expression of *TRIO* (left) and *RICTOR* (right) from each tumor tissue is plotted according to the tumor's change in copy number for the gene (2 indicating amplification and 1 indicating copy-number gain). The boxes show median and interquartile range for RNA levels; the whiskers show the range (excluding outliers) and circles show outliers. **C,** DSS among 32 patients with high *ITGA10* expression (measured by quantitative PCR) according to expression of *TRIO* and *RICTOR*. **D,** mRNA levels of *TRIO* (top), *RICTOR* (bottom) in four myxofibrosarcoma (MXF) cell lines and four cell lines of normal mesenchymal origin (hMSC, ASC, KEL-FIB, and SGBS). Bars colored dark red indicate that the corresponding gene is amplified in the cell line. **E,** levels of TRIO, RICTOR, and mTOR in the cell lines, detected by immunoblotting. Equal loading of the lanes is demonstrated by Ponceau S staining of the gel (bottom). **F,** physical association of TRIO and RICTOR with integrin-α10. Lysates from MXF8000 cells incubated on a dish coated with collagen II were collected and subjected to immunoprecipitation with antibody against integrin-α10 or control rabbit IgG. The immunoprecipitated complexes, as well as duplicate samples of the input lysate, were blotted with antibodies against integrin-α10 (mouse monoclonal), TRIO, RICTOR, or RAPTOR (arrow indicates expected position). Positive control for integrin-α10 detection was lysate from 293T cells transfected with *ITGA10* (293FT + α10).

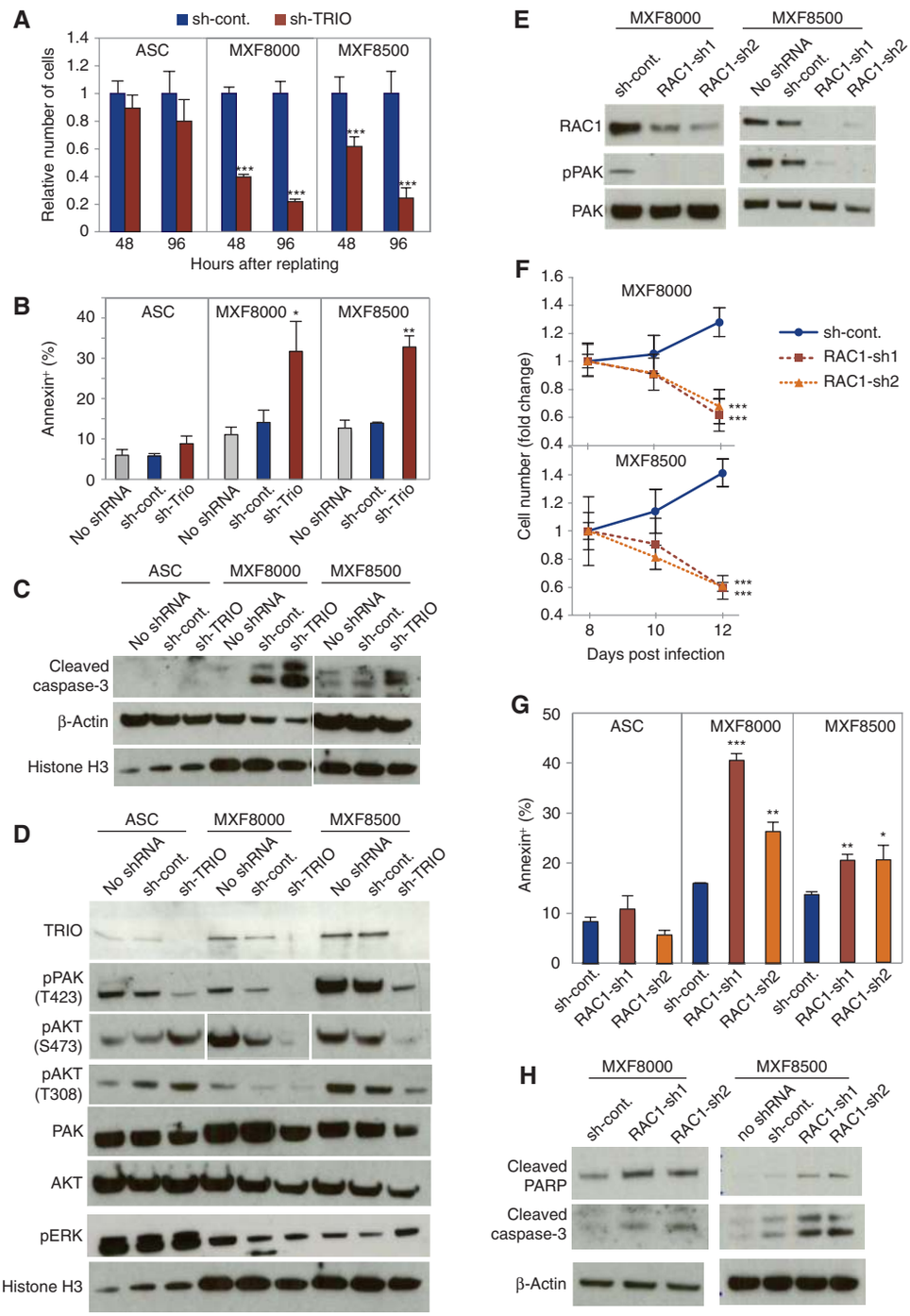

Figure 4. TRIO and RAC1 are essential for cell growth and survival for myxofibrosarcoma but not ASCs. **A–D,** knockdown of TRIO in ASCs, MXF8000, and MXF8500. Cells were infected with lentivirus carrying shRNA against TRIO; controls were lentivirus carrying control shRNA (sh-cont.) or uninfected cells (no shRNA). **A,** cell proliferation after TRIO knockdown. At 6 days after infection, equal numbers of cells were plated, then cell viability was quantified 48 and 96 hours later. The plots show fold changes relative to the control shRNA. **B** and **C,** apoptosis after TRIO knockdown. Uninfected control cells, shRNA control, or TRIO knockdown cells at infection day 10 were assessed for apoptosis by quantifying the annexin V–positive percentage (**B**) or by immunoblotting with anti-cleaved caspase-3 (**C**). **D,** effect of TRIO knockdown on signaling proteins. Cells treated as described above were subjected to immunoblotting with indicated antibodies. **E–H,** knockdown of RAC1 in myxofibrosarcoma cells (MXF8000 and MXF8500) and ASCs. **E,** effect of knockdown on levels of RAC1 and phospho-PAK (pPAK), detected by immunoblotting. **F,** cell proliferation after RAC1 knockdown. Equal numbers of cells with scramble control shRNA (sh-cont.) or *RAC1* shRNA were plated 7 days after lentivirus infection, then cell viabilities were quantified at the indicated times. The plots show fold change relative to the day of plating. **G** and **H,** apoptosis after RAC1 knockdown. Uninfected cells and cells with control shRNA or *RAC1*-knockdown shRNA at infection day 12 were assessed for apoptosis by quantifying cells positive for annexin V (**G**) or by immunoblotting with antibody to cleaved caspase-3 or cleaved PARP (**H**).

myxofibrosarcoma cells and ASCs. TRIO knockdown suppressed cell growth and induced apoptosis in myxofibrosarcoma cells but not in ASCs (Fig. 4A–C). TRIO knockdown also decreased phospho-PAK levels strongly in myxofibrosarcoma cells but only modestly in ASCs (Fig. 4D). A second shRNA, which gave less effective TRIO knockdown, also inhibited phospho-PAK and induced apoptosis, albeit at a later time point (Supplementary Fig. S5A). Two shRNAs against RAC1 decreased levels of both RAC1 and its direct target phospho-PAK (Fig. 4E; Supplementary Fig. S5B). RAC1 knockdown induced robust growth suppression (Fig. 4F) and apoptosis (Fig. 4G and H), indicating that RAC1 is essential for PAK activation and the growth and survival of myxofibrosarcoma cells. In contrast, in normal ASCs RAC1 knockdown induced modest growth suppression but not apoptosis (Supplementary Fig. S5B and S5C), indicating that RAC1 is dispensable for ASC survival. These data support the model where integrin-α10 confers a tumor-specific survival signal in myxofibrosarcoma cells at least in part through TRIO and its effector RAC. Notably, upon knockdown of TRIO, the phosphorylation of AKT at S473 and T308 was inhibited in both of the myxofibrosarcoma cell lines but not in ASCs, whereas the phosphorylation of ERK was not inhibited in any of the cell types (Fig. 4D). RAC1 knockdown in myxofibrosarcoma cells similarly inhibited phosphorylation of AKT, as well as inhibiting the phosphorylation of two mTORC1 targets: S6 and 4EBP (Supplementary Fig. S5D). These results suggest that myxofibrosarcoma cells, but not normal mesenchymal cells, have positive cross-talk between RAC/PAK and AKT pathways.

RICTOR Is Essential for Activation of AKT and Cell Growth for Myxofibrosarcoma Cells, but Not ASCs

We next assessed the role of RICTOR in the integrin-α10–mediated myxofibrosarcoma survival signal. RICTOR knockdown induced substantial growth suppression and apoptosis in myxofibrosarcoma cell lines, but not in ASCs (Fig. 5A–C), similar to the integrin-α10 knockdown phenotype. RICTOR knockdown in myxofibrosarcoma cell lines reduced phosphorylation of AKT at S473 (Fig. 5D, middle and right). RICTOR knockdown also reduced phosphorylation of mTORC1 targets S6 and 4EBP, indicating that RICTOR/mTORC2 controls mTORC1 activity in myxofibrosarcoma cells. In addition, RICTOR knockdown in myxofibrosarcoma cells downregulated phospho-T308 AKT, which is not a direct phosphorylation target of mTORC2, suggesting that RICTOR may regulate AKT partly through an mTOR-independent mechanism. Interestingly, although the extent of RICTOR knockdown was similar in normal ASCs and myxofibrosarcoma cells, knockdown in ASCs had little effect on phospho-S473 and phospho-T308 AKT, suggesting that RICTOR has no major role in AKT phosphorylation in normal mesenchymal stem cells. Furthermore, RICTOR knockdown in myxofibrosarcoma cells inhibited phosphorylation of PAK, which suggests tumor-specific cross-talk between the pathways under integrin-α10 is bidirectional.

To further test requirement for mTOR complexes, we knocked down SIN1, another essential component of mTORC2, and RAPTOR, an essential mTORC1 component. Both shRNAs against SIN1 induced growth suppression through apoptosis (Fig. 5E and F). In contrast, RAPTOR knockdown did not cause cell death in myxofibrosarcoma cells (Supplementary Fig. S6A and S6B). These results demonstrate the specific requirement of mTORC2 for myxofibrosarcoma survival.

Constitutively Active RAC, PAK, and AKT Rescue ITGA10 Knockdown-Induced Growth Suppression and Apoptosis

We next tested whether RAC1 and AKT activation can fully account for the effects of integrin-α10 on myxofibrosarcoma cell growth and survival. To do this, we tested for rescue of integrin-α10 knockdown by constitutively active mutants of RAC1 (RAC1-L61), PAK (PAK1-T423E), and AKT (Myr-AKT). MXF8000 cells were infected with lentivirus carrying either vector control or one of the constitutively active mutants, then infected with lentivirus carrying shRNA against integrin-α10. As expected, cells with control vector plus *ITGA10* shRNA underwent growth suppression and apoptosis. Expression of RAC1-L61, and to a lesser extent, expression of Myr-AKT, rescued integrin-α10–silenced cells from the apoptosis and the growth suppression (Fig. 6A and B). Expression of PAK1-T423E completely rescued the integrin-α10–silenced cells from apoptosis and mostly rescued them from growth suppression (Fig. 6A and B, right). These data suggest that active RAC1 and PAK1 are sufficient to provide a survival signal.

Pharmacologic Inhibitors of RAC and mTORC Inhibit Growth of Myxofibrosarcoma Cells *In Vitro*

We further examined the importance of TRIO/RAC and RICTOR for the survival of myxofibrosarcoma cells by using pharmacologic inhibitors.

To inhibit RAC activation by TRIO, we used two drugs: first, NSC27366 (29), which blocks the binding of RAC to guanine exchange factors, including TRIO; second, EHop-016, a newly developed derivative of NSC27366 with 100-fold lower IC_{50} toward RAC1 (30). NSC27366 and EHop-016 each robustly suppressed growth of MXF8000 cells (Fig. 6C). After 48 hours of treatment at the higher drug concentrations, cells were completely eliminated. Supporting our observation of cross-talk between RAC/PAK and AKT pathways, EHop-016 inhibited AKT activation and slightly inhibited mTORC1 (Supplementary Fig. S7A). Detection of annexin V–positive cells and cleaved caspase-3 (Fig. 6D and E) confirmed that a cause of the growth suppression was induction of apoptosis. In ASCs, treatment with either NSC23766 or EHop-016 exhibited cytostatic effects (Supplementary Fig. S7B). This growth inhibition may be explained by the fact that NSC23766 and EHop-016 inhibit RAC2 and RAC3 as well as RAC1 (30, 31). IPA3, a specific inhibitor of PAK, also induced growth suppression and apoptosis in a dose-dependent manner in myxofibrosarcoma, while it showed modest antiproliferative effects in ASCs (Fig. 6C–E; Supplementary Fig. S7B and S7C). Thus, both pharmacologic inhibition and knockdown experiments indicate that TRIO/RAC1 activities are required for the growth of myxofibrosarcoma cells.

To inhibit mTORC2, we used a selective mTOR kinase inhibitor, INK128 (MLN0128). The treatment of myxofibrosarcoma cells with INK128 for 48 or 96 hours caused dose-dependent growth suppression and induced complete growth arrest by 7 days of treatment (Fig. 6C and data not shown). However, INK128 did not induce apoptosis even at

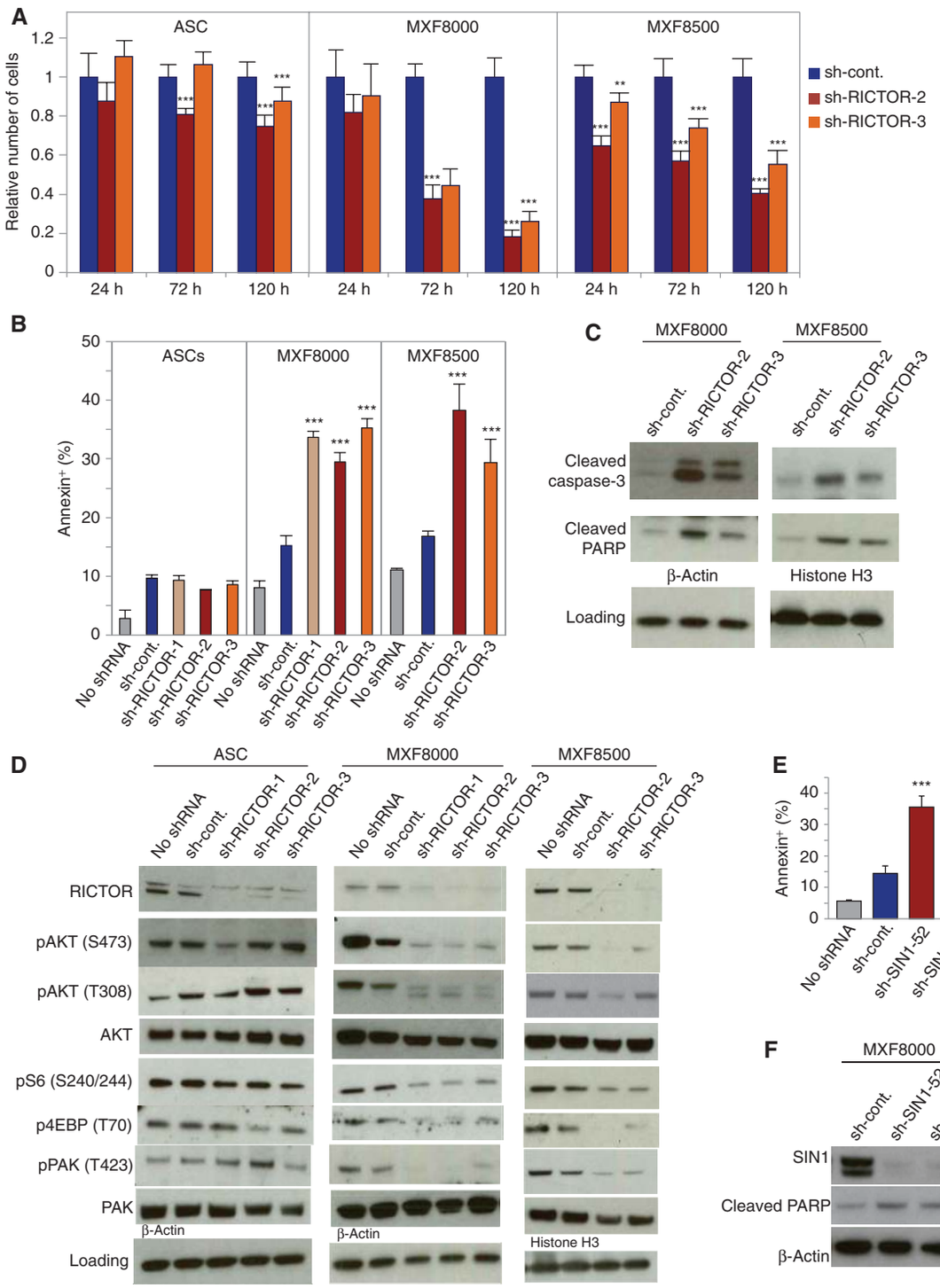

Figure 5. RICTOR is essential for cell growth, survival, and activation of AKT and PAK in myxofibrosarcoma cells, but not in ASCs. ASC, MXF8000, or MXF8500 cells were infected with lentivirus carrying control shRNA (sh-cont.) or one of three shRNAs against RICTOR. **A,** effect of RICTOR knockdown on cell proliferation. Equal numbers of cells were plated 7 days after lentivirus infection, then cell viability was determined at the indicated time points. The plots show fold changes relative to the control shRNA. **B** and **C,** RICTOR knockdown or control cells were assessed for apoptosis by detecting annexin-positive cells (**B**), or immunoblotting with antibody for cleaved caspase-3 or cleaved PARP (**C**). **D,** effect of RICTOR knockdown on signaling proteins. Uninfected cells or cells with control or *RICTOR* shRNAs were subjected to immunoblotting 10 days after infection. **E** and **F,** effect of SIN1 knockdown on apoptosis. MXF8000 cells infected with lentivirus carrying control shRNA (sh-cont.) or one of two shRNAs against *SIN1* were assessed for apoptosis by detecting annexin-positive cells (**E**) or immunoblotting with anti-cleaved PARP (**F**).

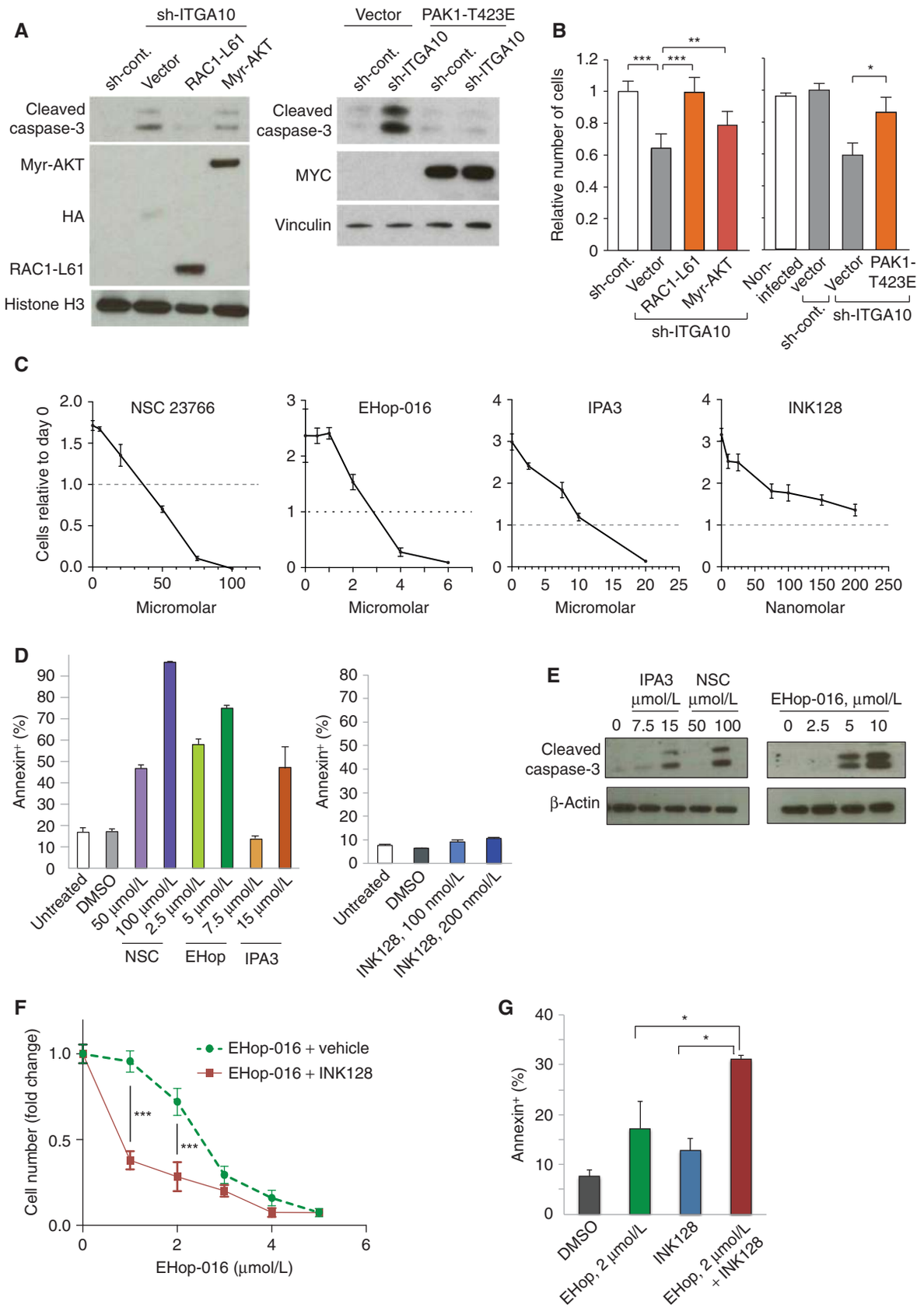

the highest dose (Fig. 6D). This is consistent with our results with Myr-AKT, which showed that activated AKT in *ITGA10*-silenced myxofibrosarcoma cells partially restored cell growth and only modestly suppressed apoptosis (Fig. 6A and B).

The fact that RICTOR knockdown affects apoptosis whereas mTOR kinase inhibition does not suggests that RICTOR has an mTOR kinase–independent role in myxofibrosarcoma cell survival. To investigate this further, we checked the effect of INK128 on the activity of various kinases by Western blot. We confirmed that INK128 reduced phosphorylation of AKT at S473 to a similar extent as we observed with RICTOR knockdown (Supplementary Fig. S7D). As expected, INK128 also caused complete inhibition of mTORC1 kinase activity, as detected by phospho-S6 and phospho-4EBP. However, unlike RICTOR knockdown, INK128 treatment did not change the level of phospho-PAK or of phospho-AKT at T308. These results suggest that RICTOR plays an additional role in the survival of myxofibrosarcoma cells independent of mTOR kinase activity, perhaps through the regulation of PAK and AKT phosphorylation at T308.

mTOR Inhibition Sensitizes Myxofibrosarcoma Cells to RAC Inhibitors

Because integrin-α10 exerts its tumor-specific growth signal through both RAC and mTORC2, we hypothesized that inhibitors of RAC and mTORC2 may have cooperative effects in myxofibrosarcoma cells.

MXF8000 cells were treated with increasing doses of EHop-016 with and without INK128 at 150 nmol/L. EHop-016 alone efficiently inhibited cell growth with an IC_{50} of 2.3 μmol/L, and in the presence of INK128 the IC_{50} of EHop-016 was reduced to 0.66 μmol/L (Fig. 6F). A similar effect was observed with a PAK inhibitor, IPA3, whose IC_{50} was reduced from 9.5 μmol/L as single agent to 2.9 μmol/L in the presence of INK128 (Supplementary Fig. S7C). In addition, the combination of low-dose EHop-016 (2 μmol/L) and INK128 resulted in significantly more apoptosis than either agent alone (Fig. 6G). These results suggest that simultaneous targeting of RAC and mTORC can achieve more efficient growth inhibition and cytotoxicity.

EHop-016 and INK128 Suppress Myxofibrosarcoma Primary and Metastatic Tumor Growth in Mouse Xenografts

We next investigated the effects of EHop-016 and INK128, alone and in combination, on myxofibrosarcoma cells xenografted into NOD/SCID gamma (NSG) mice. The myxofibrosarcoma cell line MXF8000 is tumorigenic through subcutaneous injection in NSG mice. Treatment with EHop-016 (either 15 mg/kg or 20 mg/kg twice daily by oral gavage) or INK128 (1 mg/kg daily by oral gavage) significantly inhibited tumor growth compared with the vehicle control (Fig. 7A and B). The combination of low-dose EHop-016 (15 mg/kg) and INK128 (1 mg/kg) produced still greater inhibition of primary tumor growth.

To test the efficacy of these drugs on myxofibrosarcoma metastasis, mice were injected through the tail vein with MXF8000 cells bearing a TGL reporter construct and monitored for tumor outgrowth in the lung by bioluminescent imaging. Either EHop-016 or INK128 alone significantly suppressed the lung metastasis over the time of the treatment, and again the combination of EHop-016 and INK128 more substantially inhibited the metastatic tumor growth compared with either drug administered alone (Fig. 7C). None of the treatments showed major signs of toxicity (Supplementary Fig. S8).

DISCUSSION

In myxofibrosarcoma, the development of targeted therapies has been hampered by the diversity of genomic alterations and the difficulty of distinguishing driving alterations from the vast array of passenger events. To address this problem, we performed an integrated genomic analysis of gene copy-number profiles and the transcriptome derived from 64 cases of high-grade myxofibrosarcoma and functional studies in representative patient-derived myxofibrosarcoma cell lines. These analyses identified a previously unknown but critical role of integrin-α10 for tumor growth and survival. We found that integrin-α10 acts in association with TRIO and RICTOR, which are co-amplified on 5p and overexpressed in about 50% of myxofibrosarcomas. The exquisite dependency of myxofibrosarcoma cells but not normal mesenchymal cells on integrin-α10/TRIO/RICTOR signaling circuitry represents a tumor-specific vulnerability and a promising therapeutic target, because inhibiting this circuitry can interfere with myxofibrosarcoma tumor growth and survival with minimum toxicity to normal tissues.

The most common cause of death in patients with high-grade myxofibrosarcoma is lung metastases, which occur in about 30% of patients. Presently, there are no widely used molecular predictors of distant recurrence and survival for patients with high-grade myxofibrosarcoma. However, our unsupervised clustering analysis subdivided high-grade myxofibrosarcoma into two groups that differ significantly in DSS. This molecular subgrouping can be used to identify

Figure 6. Effects of RAC modulation on myxofibrosarcoma cells *in vitro*. **A, B,** rescue of integrin-α10–knockdown phenotypes by constitutively active RAC1, AKT, and PAK1. MXF8000 cells were infected with lentivirus carrying RAC1-Q61L, myr-AKT (left), PAK1-T423E (right), or vector control, selected with blasticidin, then infected with lentivirus carrying either *ITGA10* or control shRNA. HA, hemagglutinin tag. **A,** immunoblot of cleaved caspase-3 at 8 days after the second infection (sh-ITGA10 or sh-cont.). The recombinant proteins were detected by immunoblotting with anti-HA (to detect RAC1 and AKT) and anti-MYC (to detect PAK1). **B,** cell viability assessed by Resazurin of the cells described in **A**. **C–G,** inhibitors of RAC inhibit proliferation and induce apoptosis, and an mTORC kinase inhibitor augments the effect. **C,** cell proliferation of MXF8000 cells treated at the indicated doses of each compound for 48 hours. The graphs show number of cells relative to day 0 of treatment. **D,** apoptosis assay of MXF8000 cells treated with the indicated inhibitors for 48 hours. The graphs show the mean and standard deviation of triplicate samples. **E,** immunoblot of cleaved caspase-3 in MXF8000 cells treated with the indicated doses of IPA3, NSC 23766 (NSC), or EHop-016 for 24 hours. **F,** cell proliferation assessed by CyQuant in MXF8000 cells treated with increasing doses of EHop-016 plus either INK128 (150 nmol/L) or vehicle for 48 hours. **G,** apoptosis in cells treated with INK128 (150 nmol/L), EHop-016 (EHop; 2 μmol/L), or both drugs.

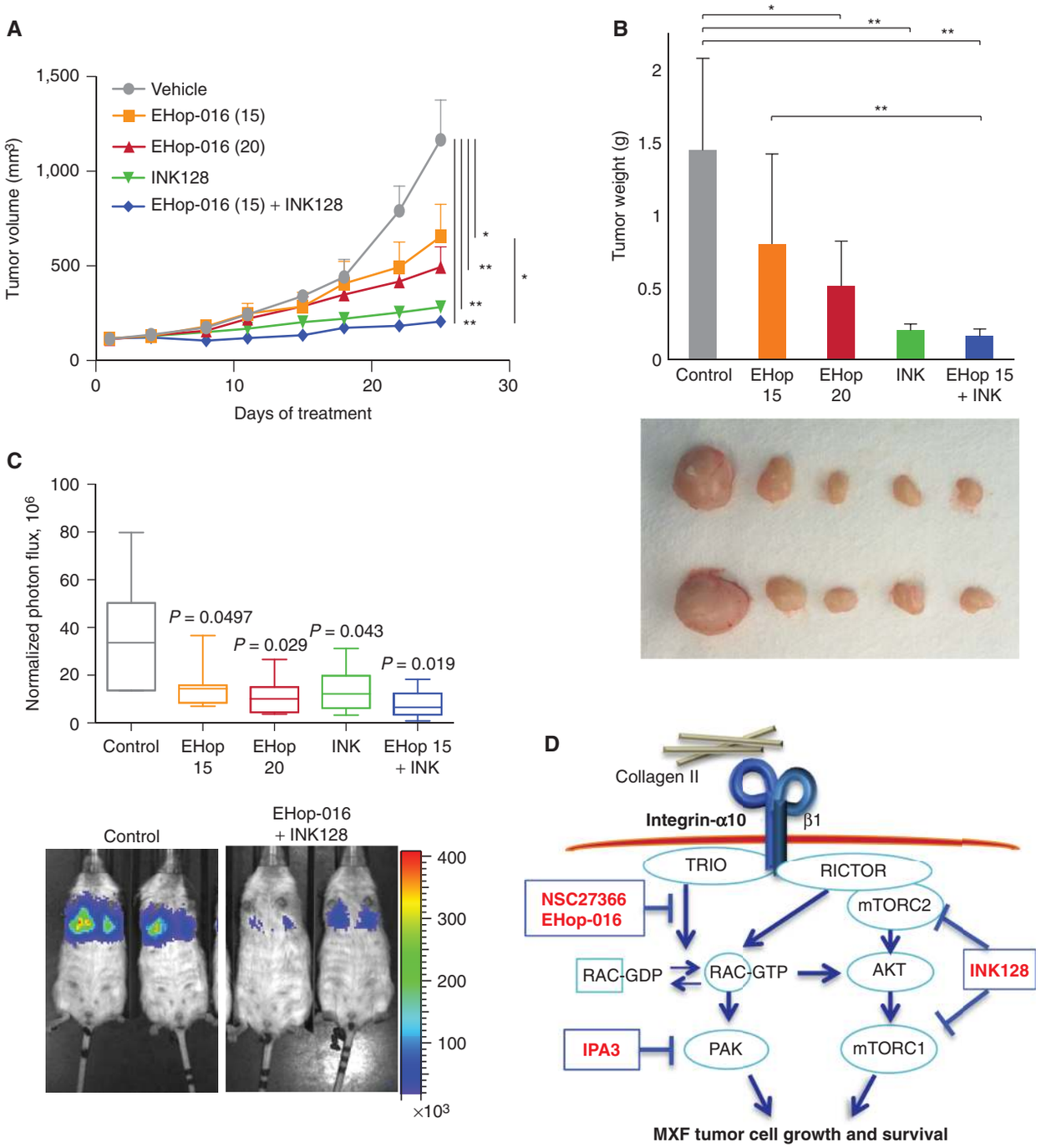

Figure 7. EHop-016 and INK128 treatment of myxofibrosarcoma xenografts in NSG mice. **A,** effects of the inhibitors on growth of subcutaneous MXF8000 xenografts. The mice were treated with vehicle, EHop-016 at 15 or 20 mg/kg, INK128 at 1 mg/kg, or EHop plus INK128. The tumor volume was monitored by caliper. **B,** tumor weight at the end of the treatment (day 28; top), and photographs of representative tumors (bottom). **C,** effects of the inhibitors on lung metastases after tail-vein injection of MXF8000 cells. Mice were treated with the same drug regimens as in **A**. Tumor in lung was measured by bioluminescent imaging at treatment day 60 (top). The bottom panel shows representative bioluminescent images of the control group and the group treated with the combination of EHop-016 and INK128. **D,** schematic model of the tumor-specific integrin-α10 pathway working through oncogenic TRIO and RICTOR toward the downstream effectors for growth and survival. Inhibitors are indicated in bold red type.

high-risk patients who might need more intense follow-up and/or treatment with neoadjuvant chemotherapy. The differentially expressed genes had a striking concentration of genes related to cell–ECM adhesion and cytoskeletal remodeling, including *ITGA10* as the gene most significantly associated with disease-specific and metastasis-free survival. The relationship between *ITGA10* expression and metastasis is also supported by the higher *ITGA10* expression in metastases than in primary tumors, including in matched samples.

Our model for the tumor-specific signaling of integrin-α10 is shown in Fig. 7D. Through genomic analysis and knockdown and biochemical studies, we demonstrate that integrin-α10 signals through TRIO to RAC and is required for PAK activation in myxofibrosarcoma cells but not in normal mesenchymal cells. This pathway is required for proliferation and survival in myxofibrosarcoma cells. By the same means, we found that integrin-α10 signals through RICTOR (in the mTORC2 complex) and that both integrin-α10 and RICTOR are required for activation of AKT and mTORC1. Integrin-α10, TRIO, RICTOR, and RAC all promote cell proliferation and transmit a prosurvival signal in myxofibrosarcoma cells but not in normal cells. Finally, constitutively active RAC, PAK, and AKT rescue the growth inhibition and apoptosis caused by integrin-α10 knockdown, demonstrating that much of integrin-α10's progrowth and prosurvival functions are carried out through these proteins. Altogether, these results uncover the novel role for integrin-α10 as a critical driver in myxofibrosarcomagenesis by controlling TRIO/RAC/PAK and RICTOR/mTORC2 pathways in a tumor-specific fashion.

Some pro-malignant integrins are known to collaborate with oncogenes, such as RAS, PI3K–AKT, SRC, FAK, MET, and ERBB2, to drive tumor initiation, invasion, or systemic dissemination (14, 15, 17, 32). Integrin-mediated signaling generally requires activation of FAK and SRC family kinases (14). Interestingly, however, our results indicate that integrin-α10 does not significantly regulate FAK or SRC in myxofibrosarcoma cells. Consistent with this, we found that high dosages of the SRC kinase inhibitor dasatinib modestly inhibited myxofibrosarcoma cell growth but did not induce apoptosis (data not shown). Integrin-mediated signaling is also known to engage in cross-talk with MET, and MET is overexpressed in a subset of myxofibrosarcomas (33). Nevertheless, integrin-α10 in myxofibrosarcoma does not seem to exert its tumorigenic effects through MET, as the MET inhibitor crizotinib was not antiproliferative or proapoptotic (data not shown). Moreover, integrin-α10 is not essential for adhesion to collagen II nor for formation of focal adhesions, which typically have concentrations of vinculin and phospho-FAK. Presumably, *ITGA10*-silenced cells can adhere using other collagen II–receptor integrins, specifically α1β1 and α2β1, both of which are expressed in myxofibrosarcoma cells (data not shown). This is consistent with the fact that *Itga10* knockout chondrocytes adhere to collagen II to the same extent as wild-type cells (20). However, integrin-α10 seems to be indispensable in mediating signaling toward RAC/PAK and AKT via complex formation with TRIO and RICTOR.

RAC is known to be significant in initiation and progression of cancers, and it is hyperactivated in a number of cancer types (34). Most commonly, RAC hyperactivation occurs through the activation of guanine exchange factors (which positively regulate RAC) or the inactivation of GTPase-activating proteins (which negatively regulate RAC; ref. 35). In myxofibrosarcoma, RAC activity is essential, whereas normal mesenchymal cells can survive without RAC1 or its guanine exchange factor TRIO. This dependency is presumably a consequence of *TRIO* gene amplification and overexpression and/or TRIO activation by integrin-α10. TRIO, an oncogenic guanine exchange factor for Rho-GTPases, can transform normal fibroblasts and is overexpressed in several cancers. TRIO plays an essential role in oncogenic Galpha(q) signaling in cervical cancer and uveal melanoma (36). TRIO also promotes cancer cell motility as part of the NOTCH and ABL signaling axis in colorectal cancer (37). In our study, blocking TRIO's ability to activate RAC with NSC23766 or EHop-016 resulted in prominent growth inhibition and cytotoxicity in myxofibrosarcoma cells. These effects occurred at dosages that suppress RAC but not CDC42, a closely related Rho-GTPase. Furthermore, EHop-016 revealed significant antitumor activity for both subcutaneous primary tumors and lung metastasis after tail-vein injection. These results, together with reports that RAC inhibitors of this class have preclinical efficacy against several tumor types (38, 39), further support the idea of targeting the TRIO/RAC axis. EHop-016 seems particularly promising for further development, because in mice it has 26% to 40% oral bioavailability and linear pharmacokinetic profiles (40). Alternatively, the pathway could be targeted with PAK inhibitors, such as IPA3.

Like RAC and TRIO, RICTOR has been implicated in several cancers (41–44). A tumor-specific function of RICTOR was demonstrated in studies using knockout mice; RICTOR was shown to be dispensable for normal prostate development but essential for the development of PTEN loss–induced prostate cancer (41). In breast cancer, RICTOR is required for ERBB2-driven tumor growth through its activation of AKT and mTORC1 (42). In both prostate and breast cancer cells, RICTOR's tumor-specific function is associated with its regulation of AKT phosphorylation at T308 as well as S473, both of which are required for mTORC1 activity in transformed cells. Similarly, in myxofibrosarcoma cells, we demonstrated that RICTOR is required for AKT phosphorylation at T308 and S473 as well as for mTORC1 activity. However, RICTOR knockdown also induced apoptosis, whereas inhibiting mTORC1 and mTORC2 with INK128 did not, suggesting that RICTOR has a prosurvival function independent of its phosphorylation of AKT. This function might be through the regulation of RAC/PAK, because RICTOR knockdown, but not INK128, suppresses phospho-PAK. This idea of cross-talk between RICTOR and RAC/PAK is consistent with reports demonstrating that RICTOR promotes RAC activity through negative regulation of RhoGDI2 or positive regulation of PREX1, a guanine exchange factor for RAC; these events promote cell migration (45, 46). In another instance of cross-talk between the two pathways, RAC and PAK are involved in activation of AKT and mTORC1 (47, 48). Similarly, we observed that TRIO or RAC1 knockdown significantly affects the activation of AKT in myxofibrosarcoma, though not in normal mesenchymal stem cells.

Inhibition of RICTOR/mTOR signaling using INK128 yielded significant antiproliferative effects *in vitro* and in mouse models of myxofibrosarcoma. Although INK128 alone does

not induce apoptosis in myxofibrosarcoma *in vitro*, it increases EHop-016–induced growth inhibition and potentiates the cytotoxicity of low-dose EHop-016. The reduced dose of EHop-016 required in the presence of INK128 would help reduce any adverse effects on normal cells. INK128 as single agent showed efficient antitumor effects *in vivo* for primary tumor growth as well as lung metastases. Indeed, INK128 has demonstrated antitumor effects against various sarcoma models, including rhabdomyosarcoma and Ewing sarcoma xenografts and liposarcoma cell lines (49). It is currently in phase II clinical trials for several cancers. Our data suggest that patients with myxofibrosarcomas at high risk for metastasis could benefit from INK128. Importantly, the antitumor effects on both primary tumor and lung metastases were greatest with the combination of EHop-016 and INK128, supporting our hypothesis that integrin-α10–mediated TRIO/RAC signaling and RICTOR signaling represent promising therapeutic targets. These results have led to the inclusion of patients with myxofibrosarcoma or undifferentiated pleomorphic sarcoma in an ALLIANCE-sponsored phase I/II study of INK128 (MLN0128) versus pazopanib in patients with advanced sarcoma.

Integrin-α10 itself is an attractive therapeutic target. In adults, its expression is restricted to cartilage, limiting the risk of toxicity of integrin-α10–targeted agents (19). No direct inhibitor for integrin-α10 is currently available. However, because integrin-α10 is on the cell surface, it could plausibly be targeted using chimeric antigen receptor T-cell immunotherapy (50) or agents that interfere with integrin-α10's ligand binding, such as a ligand–mimetic peptide or a monoclonal antibody against its I-domain (51).

Altogether, this study shows that integrin-α10 plays a pivotal role for pathogenesis of myxofibrosarcoma via tumor-specific control of TRIO/RAC and RICTOR signaling and thus uncovers novel possible therapeutic options to treat patients with aggressive or metastatic myxofibrosarcomas.

METHODS

Patients

The study cohort was drawn from patients operated on for high-grade untreated primary myxofibrosarcoma at Memorial Sloan Kettering Cancer Center (MSKCC) between January 2002 and March 2011. We screened all patients with untreated primary tumors diagnosed as either myxofibrosarcoma or malignant fibrous histiocytoma who gave consent for tissue banking ($N = 106$). Every case was reviewed by a sarcoma pathologist (N. Agaram) and assigned a percent myxoid component; 36 tumors were excluded for having <10% myxoid component or insufficient slides to assess myxoid component. All patients who met these criteria and had enough banked RNA-quality tissue were included in this study ($n = 64$). The study was approved by MSKCC's institutional review board (IRB; protocol #02-060) and was conducted in accordance with the Declaration of Helsinki. All patients gave informed consent. Data for each patient on diagnosis, treatment, time to local/distant recurrence, and survival were retrieved from a prospectively maintained database.

RNA Isolation and Microarray Analysis

RNA was isolated from tumor tissues as described (52). Briefly, tissues from cryomolds were reviewed by a sarcoma pathologist (N. Agaram), and areas of necrosis or normal tissue were removed by macrodissection. The tumor tissues were lysed in QIAzol lysis reagent and homogenized using Mixer Mill MM 300 (Retsch). RNA was purified using the RNeasy Lipid Tissue Mini Kit (Qiagen). For tissue culture cells, total RNA was extracted using the RNeasy Kit (Qiagen). cDNA preparation and U133A microarray analysis were performed as described (53). The microarray data are available from GEO (accession number GSE72545).

Statistical Analysis

Affymetrix U133A microarray data for 118 myxofibrosarcoma arrays (including the 64 high-grade myxofibrosarcomas that were the focus of this study), 22 normal fat arrays, and 11 normal muscle arrays were preprocessed using the Robust Multi-Array Average method as implemented by the just.rma function in the R affy package (54). Preprocessed data from the 64 high-grade myxofibrosarcoma arrays with and without the data from the normal fat and muscle arrays were then subjected to clustering using the consensus clustering method (55), which uses bootstrapping to create repeated random samples of the data, calculates the frequency of co-clustering between each array pair across the bootstrap samples, and then uses one minus the co-clustering frequency as the distance measure and the Ward link function for clustering the arrays. The identified myxofibrosarcoma clusters were compared with clinical outcomes using the Kaplan–Meier curve and Cox proportional hazards regression. Signature genes for the clusters were selected by comparing the expression level of each gene between the clusters using the LIMMA method (56) and a stringent *P*-value cutoff of 10^{-6} (to account for the fact that the clustering was based on the same microarray data). The association between the gene expression (as a continuous variable) and DSS was evaluated using the Cox proportional hazards regression and the score test (57). A *P*-value cutoff of 0.005 was used to select significant prognostic gene probes. Among the 2,366 probes that distinguish the two clusters, about 12 probes are expected to have such a small *P* value just by chance. Expression was dichotomized at the median (for *ITGA10*) or at the upper quartile (for *TRIO* and *RICTOR*) for generating Kaplan–Meier curves. On the experimental studies, data are presented as mean ± standard deviation. The Student *t* test (unpaired, two-tailed) was used to compare two groups for independent samples.

Pathway and Gene Annotation Analysis

Genes that were both part of the cluster signature and associated with DSS (146 genes) were analyzed with the NetBox algorithm using default parameters: Human Interaction Network, shortest path length of 2, and an FDR-adjusted *P*-value threshold for linker gene inclusion of 0.05 (26). The identified modules with five or more members were analyzed individually for functional annotation enrichment with the DAVID tool (27).

Copy-Number Analysis

Copy number was analyzed by array CGH in tumor tissue from the 64 study patients. Preparation of DNA, analysis on Agilent 244K or 1M arrays, and data analysis were as described (58). For each gene of interest, copy-number change was called as −2, −1, 0, 1, or 2 (deletion, loss, no change, gain, amplification). Association between copy number and mRNA level was assessed by the Kruskal–Wallis rank-sum test.

Cell Culture and Reagents

Following guidelines in IRB-approved protocol 02-060, primary myxofibrosarcoma cell lines (MXF8500, MXF2734, MXF8000, and MXF9100) were derived during 2004 to 2011 from fresh human primary myxofibrosarcoma tumor samples using collagenase digestion and established in cell culture. Array CGH was performed on all primary cell lines and compared with array CGH performed on the human tumor tissue from which they were derived in order to verify

that the copy-number alterations in the cell lines were representative of those found in the original tumor samples. The cell lines were last tested in 2014.

ASCs were a generous gift from Dr. Jeffrey M. Gimble, and SGBS cells were a generous gift from Dr. Martin Wabitsch. Umbilical cord–derived human mesenchymal stem cells and human dermal fibroblast cells (KEL-FIB) were from ATCC. All cells were grown in a 50:50 mixture of Dulbecco's Modified Eagle Medium (DMEM) high glucose and F12 medium (DMEM HG/F12) with 10% fetal bovine serum, 2 mmol/L L-glutamine, 100 units/mL penicillin, and 100 μg/mL streptomycin and maintained in a 37°C incubator with 5% CO_2. Collagen I was from Sigma and collagen II from Millipore. NSC23766 and INK128 were obtained from Cayman, EHop-016 from Millipore and Selleckchem, and IPA3 from Tocris.

Lentiviral Transduction for shRNA and Gene Expression

Human pLKO.1 lentiviral shRNAs were from Thermo Scientific Open BioSystems. The clones used were as follows: *ITGA10* (TRCN0000057725 and TRCN0000057726), *ITGA1* (TRCN0000057748 and TRCN 0000057749), *ITGA2* (TRCN0000057731 and TRCN0000308081), *TRIO* (TRCN0000010561 and GIPZ, V2LHS_1430), *RAC1* (TRCN 0000318430, TRCN0000318375, and TRCN0000004870), *RICTOR* (TRCN0000074288, TRCN0000074289, and TRCN0000074290), *SIN1* (TRCN0000003152 and TRCN0000003153), and *RAPTOR* (TRCN0000039770 and TRCN0000039772). Viral particles were generated in HEK293T cells (ATCC) as described (53). HA-RAC1 was subcloned into pLOC (Open Biosystems), and the constitutively active mutation (Q61L) was introduced by QuickChange Site-Directed Mutagenesis (STRATAGENE). Myristoylated HA-tagged AKT1 was subcloned from pCDH-Myr-AKT1-puro (Addgene) into pLOC (Open Biosystems). PAK1T423E was obtained from Addgene (#12208) and subcloned into pLOC. The lentivirus construct bearing ITGA10 (pLV151) was from Genecopoeia.

Cell Proliferation and Apoptosis

Cell proliferation was assessed in sextuplicate cultures using Resazurin dye (Acros Organics) or CyQuant Cell Proliferation Kit (Invitrogen) as described (52, 59). Resazurin (50 μmol/L) was added to each well at the time points noted, and plates were incubated at 37°C for 24 hours, then subjected to measurement of fluorescence (excitation/emission 555/585 nm). Plates were read using SoftMax Pro v5.4.1 software and the SpectraMax M4 plate reader (Molecular Devices). Evaluation of apoptosis was carried out in triplicate cultures using Muse Annexin V and Dead Cell Assay Kit (Millipore) following the manufacturer's protocol on the MUSE cell analyzer (Millipore).

Migration and Matrigel Invasion

Cells were trypsinized, resuspended in serum-free medium, and then applied to Transwell inserts (8-μm pore size; BD Falcon) in 24-well plates. Inserts were either noncoated (migration assay) or coated with 5 μg of Matrigel (invasion assay). Serum-containing medium was placed in the bottom chamber. Eighteen hours later, cells that had reached to the bottom were fixed, stained with crystal violet, and counted.

Western Blotting

Cells were lysed in high SDS lysis buffer (2.5% SDS, 62.5 mmol/L Tris–HCl pH 6.8, 10% glycerol) and immediately boiled to denature proteins. Protein concentration was determined using the DC Protein Assay (BioRad Laboratories). Cell lysate was resolved on a NuPAGE Novex 3% to 8% Tris-acetate gel or 4% to 12% Bis-Tris gel (Invitrogen) in the XCell SureLock MiniCell (Invitrogen), and then transferred to the nitrocellulose membrane (Millipore). Membranes were blocked and incubated with antibodies in Starting Block T20 (Thermo Scientific).

We generated the anti–integrin-α10 mouse monoclonal antibody using as immunogen a peptide sequence within the predicted ligand-binding surface of the I-domain (avoiding sequence shared with ITGA1 and ITGA2; NeoBio). The commercial antibodies and sources are listed in Supplementary Table S6.

Biochemistry

For the coimmunoprecipitation and collagen II–induced signaling experiments, MXF8000 cells were detached using enzyme-free detachment medium (Gibco) and kept in suspension in serum-free medium with 2% BSA for 30 minutes, then replated on dishes precoated with collagen II (Millipore) at 10 μg/mL. Cells were harvested three hours later (for immunoprecipitations) or at the times indicated in the figure. For immunoprecipitations, total lysates were prepared in lysis buffer [20 mmol/L Tris–HCL, 150 mmol/L NaCl, 1% Triton-X100, 5 mmol/L $MgCl_2$, 1 mmol/L EDTA, proteinase inhibitor cocktail (SIGMA), and phosSTOP tablet (Roche)]. Lysate was subjected to immunoprecipitation using anti–integrin-α10 (AB6030) or rabbit IgG (SIGMA), then immunocomplexes were subjected to Western blotting using anti–integrin-α10 monoclonal antibody (Neobio).

GTP-RAC was assessed using a GST-PBD pulldown assay as described (60).

Collagen Adhesion

Cells were detached using enzyme-free detachment medium (Gibco), then resuspended in serum-free medium with 2% BSA. Fifteen thousand cells were replated on 96-well plates precoated with 1% BSA, collagen I, or collagen II (10 μg/mL) for 50 minutes. The plates were washed, then attached cells were fixed with 4% paraformaldehyde and stained with 0.1% crystal violet. After overnight treatment with 0.5% Triton-X100, optical density of the plates was read at 595 nm.

Mouse Tumorigenicity and Metastasis

All animal experiments were done in accordance with a protocol approved by the MSKCC Institutional Animal Care and Use Committee. MXF8000 cells (2 million, suspended in PBS and Matrigel at 1:1) were injected subcutaneously into female NSG mice (age 6–8 weeks). Drug treatments started when tumors reached approximately 100 mm^3. Mice (6 per group) were treated by oral gavage 5 days per week with the following: (i) vehicle; (ii) EHop-016, 15 mg/kg; (iii) EHop-016, 20 mg/kg; (iv) INK128, 1 mg/kg; (v) EHop-016, 15 mg/kg plus INK128, 1 mg/kg. EHop doses were given twice a day and INK128 once a day. The solvent was 1.2% acetic acid in PBS for EHop-016, and 5% 1-methyl-2-pyrrolidinone, 15% polyvinylpyrrolidone in water for INK128. Tumor volumes were measured by caliper twice a week. For lung colonization experiments, 2 million MXF8000 cells transduced with TGL vector were injected in the tail vein of female NSG mice (age 6–8 weeks). Mice were monitored by bioluminescence imaging (IVIS). Four weeks after injection, mice were grouped into five cohorts (8 mice each) with similar signal intensity and subjected to the same treatments as in the subcutaneous tumor experiment.

Disclosure of Potential Conflicts of Interest

No potential conflicts of interest were disclosed.

Authors' Contributions

Conception and design: T. Okada, A.Y. Lee, L.-X. Qin, S. Singer

Development of methodology: T. Okada, A.Y. Lee, Y. Shen, C. Sander, S. Singer

Acquisition of data (provided animals, acquired and managed patients, provided facilities, etc.): T. Okada, A.Y. Lee, N. Agaram, T. Mimae, R. O'Connor, M.A. López-Lago, A. Craig, F. Shima, S. Singer

Analysis and interpretation of data (e.g., statistical analysis, biostatistics, computational analysis): T. Okada, A.Y. Lee, L.-X. Qin,

Y. Shen, M.A. López-Lago, M.L. Miller, P. Agius, E. Molinelli, N.D. Socci, A.M. Crago, C. Sander, S. Singer
Writing, review, and/or revision of the manuscript: T. Okada, A.Y. Lee, L.-X. Qin, R. O'Connor, M.L. Miller, A.M. Crago, S. Singer
Administrative, technical, or material support (i.e., reporting or organizing data, constructing databases): T. Okada, Y. Shen, R. O'Connor, A. Craig, F. Shima, S. Singer
Study supervision: T. Okada, S. Singer

Acknowledgments

We thank the following individuals: Martin Wabitsch (University of Ulm) and Jeffrey Gimble (Tulane University) for cell lines; Janet Novak for editing; Alexandra Stepanovic, David Tong, and members of the Singer lab for help and discussion; and Lucile Crozet and Frederick Geissmann for help with FACS and discussion. We also thank Darren Veach and the Antitumor Assessment Core for assistance in mouse experiments. Finally, we thank Filippo Giancotti (Sloan Kettering Institute) for review of the manuscript and discussion.

Grant Support

This work was supported by the SPORE in Soft Tissue Sarcoma (P50 CA140146, to S. Singer, L.-X. Qin, and C. Sander), by the MSK Cancer Center Support Grant/Core Grant (P30 CA008748), and by donations from the Siskind Family Sarcoma Fund and the MFH Research Fund.

The costs of publication of this article were defrayed in part by the payment of page charges. This article must therefore be hereby marked *advertisement* in accordance with 18 U.S.C. Section 1734 solely to indicate this fact.

Received December 17, 2015; revised August 24, 2016; accepted August 25, 2016; published OnlineFirst August 30, 2016.

REFERENCES

1. Fletcher C, Unni K, Mertens F, editors. Pathology and Genetics of Tumors of Soft Tissue and Bone. Lyon: International Agency for Research on Cancer Press; 2002.
2. Fletcher CD, Gustafson P, Rydholm A, Willen H, Akerman M. Clinicopathologic re-evaluation of 100 malignant fibrous histiocytomas: prognostic relevance of subclassification. J Clin Oncol 2001;19:3045–50.
3. Hollowood K, Fletcher CD. Malignant fibrous histiocytoma: morphologic pattern or pathologic entity? Semin Diagn Pathol 1995;12:210–20.
4. Lee AY, Agaram NP, Qin LX, Kuk D, Curtin C, Brennan MF, et al. Optimal percent myxoid component to predict outcome in high-grade myxofibrosarcoma and undifferentiated pleomorphic sarcoma. Ann Surg Oncol 2016;23:818–25.
5. Huang HY, Lal P, Qin J, Brennan MF, Antonescu CR. Low-grade myxofibrosarcoma: a clinicopathologic analysis of 49 cases treated at a single institution with simultaneous assessment of the efficacy of 3-tier and 4-tier grading systems. Hum Pathol 2004;35:612–21.
6. Mentzel T, Calonje E, Wadden C, Camplejohn RS, Beham A, Smith MA, et al. Myxofibrosarcoma. Clinicopathologic analysis of 75 cases with emphasis on the low-grade variant. Am J Surg Pathol 1996;20:391–405.
7. Merck C, Angervall L, Kindblom LG, Oden A. Myxofibrosarcoma. A malignant soft tissue tumor of fibroblastic-histiocytic origin. A clinicopathologic and prognostic study of 110 cases using multivariate analysis. Acta Pathol Microbiol Immunol Scand Suppl 1983;282:1–40.
8. Barretina J, Taylor BS, Banerji S, Ramos AH, Lagos-Quintana M, Decarolis PL, et al. Subtype-specific genomic alterations define new targets for soft-tissue sarcoma therapy. Nat Genet 2010;42:715–21.
9. Gibault L, Perot G, Chibon F, Bonnin S, Lagarde P, Terrier P, et al. New insights in sarcoma oncogenesis: a comprehensive analysis of a large series of 160 soft tissue sarcomas with complex genomics. J Pathol 2011;223:64–71.
10. Taylor BS, Barretina J, Maki RG, Antonescu CR, Singer S, Ladanyi M. Advances in sarcoma genomics and new therapeutic targets. Nat Rev Cancer 2011;11:541–57.
11. Li CF, Fang FM, Lan J, Wang JW, Kung HJ, Chen LT, et al. AMACR amplification in myxofibrosarcomas: a mechanism of overexpression that promotes cell proliferation with therapeutic relevance. Clin Cancer Res 2014;20:6141–52.
12. Li CF, Wang JM, Kang HY, Huang CK, Wang JW, Fang FM, et al. Characterization of gene amplification-driven SKP2 overexpression in myxofibrosarcoma: potential implications in tumor progression and therapeutics. Clin Cancer Res 2012;18:1598–610.
13. Teicher BA. Searching for molecular targets in sarcoma. Biochem Pharmacol 2012;84:1–10.
14. Guo W, Giancotti FG. Integrin signalling during tumour progression. Nat Rev Mol Cell Biol 2004;5:816–26.
15. Seguin L, Desgrosellier JS, Weis SM, Cheresh DA. Integrins and cancer: regulators of cancer stemness, metastasis, and drug resistance. Trends Cell Biol 2015;25:234–40.
16. Pylayeva Y, Gillen KM, Gerald W, Beggs HE, Reichardt LF, Giancotti FG. Ras- and PI3K-dependent breast tumorigenesis in mice and humans requires focal adhesion kinase signaling. J Clin Invest 2009;119:252–66.
17. Desgrosellier JS, Cheresh DA. Integrins in cancer: biological implications and therapeutic opportunities. Nat Rev Cancer 2010;10:9–22.
18. Camper L, Hellman U, Lundgren-Akerlund E. Isolation, cloning, and sequence analysis of the integrin subunit alpha10, a beta1-associated collagen binding integrin expressed on chondrocytes. J Biol Chem 1998;273:20383–9.
19. Lundgren-Akerlund E, Aszodi A. Integrin alpha10beta1: a collagen receptor critical in skeletal development. Adv Exp Med Biol 2014;819:61–71.
20. Bengtsson T, Aszodi A, Nicolae C, Hunziker EB, Lundgren-Akerlund E, Fassler R. Loss of alpha10beta1 integrin expression leads to moderate dysfunction of growth plate chondrocytes. J Cell Sci 2005;118:929–36.
21. Wenke AK, Kjellman C, Lundgren-Akerlund E, Uhlmann C, Haass NK, Herlyn M, et al. Expression of integrin alpha10 is induced in malignant melanoma. Cell Oncol 2007;29:373–86.
22. Engel BE, Welsh E, Emmons MF, Santiago-Cardona PG, Cress WD. Expression of integrin alpha 10 is transcriptionally activated by pRb in mouse osteoblasts and is downregulated in multiple solid tumors. Cell Death Dis 2013;4:e938.
23. Dewan V, Darbyshire A, Sumathi V, Jeys L, Grimer R. Prognostic and survival factors in myxofibrosarcomas. Sarcoma 2012;2012:830879.
24. Look Hong NJ, Hornicek FJ, Raskin KA, Yoon SS, Szymonifka J, Yeap B, et al. Prognostic factors and outcomes of patients with myxofibrosarcoma. Ann Surg Oncol 2013;20:80–6.
25. Sanfilippo R, Miceli R, Grosso F, Fiore M, Puma E, Pennacchioli E, et al. Myxofibrosarcoma: prognostic factors and survival in a series of patients treated at a single institution. Ann Surg Oncol 2011;18:720–5.
26. Cerami E, Demir E, Schultz N, Taylor BS, Sander C. Automated network analysis identifies core pathways in glioblastoma. PLoS One 2010;5:e8918.
27. Dennis G Jr, Sherman BT, Hosack DA, Yang J, Gao W, Lane HC, et al. DAVID: database for annotation, visualization, and integrated discovery. Genome Biol 2003;4:P3.
28. Papaemmanuil E, Gerstung M, Bullinger L, Gaidzik VI, Paschka P, Roberts ND, et al. Genomic classification and prognosis in acute myeloid leukemia. N Engl J Med 2016;374:2209–21.
29. Gao Y, Dickerson JB, Guo F, Zheng J, Zheng Y. Rational design and characterization of a Rac GTPase-specific small molecule inhibitor. Proc Natl Acad Sci U S A 2004;101:7618–23.
30. Montalvo-Ortiz BL, Castillo-Pichardo L, Hernandez E, Humphries-Bickley T, De la Mota-Peynado A, Cubano LA, et al. Characterization of EHop-016, novel small molecule inhibitor of Rac GTPase. J Biol Chem 2012;287:13228–38.
31. Akbar H, Cancelas J, Williams DA, Zheng J, Zheng Y. Rational design and applications of a Rac GTPase-specific small molecule inhibitor. Methods Enzymol 2006;406:554–65.

32. Guo W, Pylayeva Y, Pepe A, Yoshioka T, Muller WJ, Inghirami G, et al. Beta 4 integrin amplifies ErbB2 signaling to promote mammary tumorigenesis. Cell 2006;126:489–502.
33. Lee JC, Li CF, Fang FM, Wang JW, Jeng YM, Yu SC, et al. Prognostic implication of MET overexpression in myxofibrosarcomas: an integrative array comparative genomic hybridization, real-time quantitative PCR, immunoblotting, and immunohistochemical analysis. Mod Pathol 2010;23:1379–92.
34. Vega FM, Ridley AJ. Rho GTPases in cancer cell biology. FEBS Lett 2008;582:2093–101.
35. Wertheimer E, Gutierrez-Uzquiza A, Rosemblit C, Lopez-Haber C, Sosa MS, Kazanietz MG. Rac signaling in breast cancer: a tale of GEFs and GAPs. Cell Signal 2012;24:353–62.
36. Vaque JP, Dorsam RT, Feng X, Iglesias-Bartolome R, Forsthoefel DJ, Chen Q, et al. A genome-wide RNAi screen reveals a Trio-regulated Rho GTPase circuitry transducing mitogenic signals initiated by G protein-coupled receptors. Mol Cell 2013;49:94–108.
37. Sonoshita M, Itatani Y, Kakizaki F, Sakimura K, Terashima T, Katsuyama Y, et al. Promotion of colorectal cancer invasion and metastasis through activation of NOTCH-DAB1-ABL-RHOGEF protein TRIO. Cancer Discov 2015;5:198–211.
38. Castillo-Pichardo L, Humphries-Bickley T, De La Parra C, Forestier-Roman I, Martinez-Ferrer M, Hernandez E, et al. The Rac inhibitor EHop-016 inhibits mammary tumor growth and metastasis in a nude mouse model. Transl Oncol 2014;7:546–55.
39. Martin H, Mali RS, Ma P, Chatterjee A, Ramdas B, Sims E, et al. Pak and Rac GTPases promote oncogenic KIT-induced neoplasms. J Clin Invest 2013;123:4449–63.
40. Humphries-Bickley T, Castillo-Pichardo L, Corujo-Carro F, Duconge J, Hernandez-O'Farrill E, Vlaar C, et al. Pharmacokinetics of Rac inhibitor EHop-016 in mice by ultra-performance liquid chromatography tandem mass spectrometry. J Chromatogr B Analyt Technol Biomed Life Sci 2015;981–982:19–26.
41. Guertin DA, Stevens DM, Saitoh M, Kinkel S, Crosby K, Sheen JH, et al. mTOR complex 2 is required for the development of prostate cancer induced by Pten loss in mice. Cancer Cell 2009;15:148–59.
42. Lin MC, Rojas KS, Cerione RA, Wilson KF. Identification of mTORC2 as a necessary component of HRG/ErbB2-dependent cellular transformation. Mol Cancer Res 2014;12:940–52.
43. Masui K, Tanaka K, Ikegami S, Villa GR, Yang H, Yong WH, et al. Glucose-dependent acetylation of Rictor promotes targeted cancer therapy resistance. Proc Natl Acad Sci U S A 2015;112:9406–11.
44. Cheng H, Zou Y, Ross JS, Wang K, Liu X, Halmos B, et al. RICTOR amplification defines a novel subset of patients with lung cancer who may benefit from treatment with mTORC1/2 inhibitors. Cancer Discov 2015;5:1262–70.
45. Agarwal NK, Chen CH, Cho H, Boulbes DR, Spooner E, Sarbassov DD. Rictor regulates cell migration by suppressing RhoGDI2. Oncogene 2013;32:2521–6.
46. Hernandez-Negrete I, Carretero-Ortega J, Rosenfeldt H, Hernandez-Garcia R, Calderon-Salinas JV, Reyes-Cruz G, et al. P-Rex1 links mammalian target of rapamycin signaling to Rac activation and cell migration. J Biol Chem 2007;282:23708–15.
47. Higuchi M, Onishi K, Kikuchi C, Gotoh Y. Scaffolding function of PAK in the PDK1-Akt pathway. Nat Cell Biol 2008;10:1356–64.
48. Saci A, Cantley LC, Carpenter CL. Rac1 regulates the activity of mTORC1 and mTORC2 and controls cellular size. Mol Cell 2011;42:50–61.
49. Slotkin EK, Patwardhan PP, Vasudeva SD, de Stanchina E, Tap WD, Schwartz GK. MLN0128, an ATP-competitive mTOR kinase inhibitor with potent in vitro and in vivo antitumor activity, as potential therapy for bone and soft-tissue sarcoma. Mol Cancer Ther 2015;14:395–406.
50. Fu X, Rivera A, Tao L, Zhang X. Genetically modified T cells targeting neovasculature efficiently destroy tumor blood vessels, shrink established solid tumors and increase nanoparticle delivery. Int J Cancer 2013;133:2483–92.
51. Brennan M, Cox D. The therapeutic potential of I-domain integrins. Adv Exp Med Biol 2014;819:157–78.
52. Singer S, Socci ND, Ambrosini G, Sambol E, Decarolis P, Wu Y, et al. Gene expression profiling of liposarcoma identifies distinct biological types/subtypes and potential therapeutic targets in well-differentiated and dedifferentiated liposarcoma. Cancer Res 2007;67:6626–36.
53. Gobble RM, Qin LX, Brill ER, Angeles CV, Ugras S, O'Connor RB, et al. Expression profiling of liposarcoma yields a multigene predictor of patient outcome and identifies genes that contribute to liposarcomagenesis. Cancer Res 2011;71:2697–705.
54. Irizarry RA, Hobbs B, Collin F, Beazer-Barclay YD, Antonellis KJ, Scherf U, et al. Exploration, normalization, and summaries of high density oligonucleotide array probe level data. Biostatistics 2003;4:249–64.
55. Monti S, Tamayo P, Mesirov J, Golub T. Consensus clustering: A resampling-based method for class discovery and visualization of gene expression microarray data. Mach Learn 2003;52:91–118.
56. Smyth GK. Linear models and empirical bayes methods for assessing differential expression in microarray experiments. Stat Appl Genet Mol Biol 2004;3:Article3.
57. Kalbfleisch JD, Prentice RL. The Statisical Analysis of Failure Time Data. Hoboken, NJ: Wiley; 2002.
58. Crago AM, Socci ND, DeCarolis P, O'Connor R, Taylor BS, Qin LX, et al. Copy number losses define subgroups of dedifferentiated liposarcoma with poor prognosis and genomic instability. Clin Cancer Res 2012;18:1334–40.
59. Borra RC, Lotufo MA, Gagioti SM, Barros Fde M, Andrade PM. A simple method to measure cell viability in proliferation and cytotoxicity assays. Braz Oral Res 2009;23:255–62.
60. Knaus UG, Bamberg A, Bokoch GM. Rac and Rap GTPase activation assays. Methods Mol Biol 2007;412:59–67.